Journal of Materials Chemistry C

ROYAL SOCIETY OF CHEMISTRY

PAPER

View Article Online
View Journal | View Issue

Cite this: J. Mater. Chem. C, 2023, 11, 10069

Stretchable superhydrophobic elastomers with on-demand tunable wettability for droplet manipulation and multi-stage reaction†

Xiaohong Ding, [abc] Yunchi Cai,[bd] Guofei Lu,[b] Jiapeng Hu,[b] Jinyun Zhao,[b] Longhui Zheng, [a] Zixiang Weng, [a] Huanyu Cheng, *[c] Jing Lin*[d] and Lixin Wu *[a]

Received 15th May 2023,
Accepted 25th June 2023

DOI: 10.1039/d3tc01666h

rsc.li/materials-c

Superhydrophobic surfaces with tunable wettability are critical for miniaturized reaction systems with promising applications in point-of-care diagnostics, liquid droplet micro-reactors, non-loss manipulation, and surface-enhanced Raman scattering sensing. However, the design and demonstration of stretchable superhydrophobic surfaces with on-demand transitions in wettability remain challenging. In this study, we report a facile approach to fabricating stretchable superhydrophobic surfaces with different microstructures (arc-shaped or V-shaped air pockets) for multi-stage liquid droplet micro-reactors. The surfaces with arc-shaped air pockets are kept in the stable Cassie–Baxter state enabling droplet micro-reactions, whereas the surfaces with V-shaped air pockets that go through pressure-induced Cassie–Baxter to Wenzel transitions facilitate the transport of droplets in between reactions. The low-cost and scalable fabrication method with the effective design strategy provided by this work also paves the way for broad applications that range from liquid droplet micro-reactors and manipulations to chemical detection and analysis in stretchable microfluidic devices.

1. Introduction

Surfaces with tunable wettability have attracted increasing attention because of their broad range of applications in biomedical analysis devices,[1–4] droplet transportation and water collection/harvesting,[5] droplet reactions,[6,7] water condensation,[8,9] and microfluidic devices.[10,11] Nature has inspired humans to mimic the microstructures from the skin of animals or plant surfaces to achieve versatile wettability.[6,12–14] The Cassie–Baxter state or superhydrophobic (SH) state that is manifested in the lotus effect[15,16] exhibits extraordinarily weak water adhesive forces resulting in the roll off of water droplets for self-cleaning and drag-reduction. By contrast, the Wenzel state in the rose-petal effect[17,18] provides high water adhesive forces, enabling the capture and transport of small water droplets. Although Cassie–Baxter (CB) and Wenzel (W) states are very different in their adhesive properties,[19,20] irreversible transitions can be induced from the former to the latter, with a loss of the superhydrophobicity.[19] Although reversible CB-to-W surfaces under external stimuli have been developed for droplet manipulation,[21–23] the stability of the surface wettability over time is far from sufficient for many applications, such as chemical or biochemical droplet reactions.[24,25] For multi-stage reaction/analysis, non-loss transportation of the droplet is often required in between the stages as well.

Soft and stretchable elastomers such as polydimethylsiloxane (PDMS) have been used widely in flexible biomedical sensors,[2,26] artificial e-skins,[27] and stretchable electrodes.[28] PDMS is transparent, biocompatible, chemically inert, and has good mechanical flexibility. These characteristics make PDMS an ideal choice for fabricating stretchable superhydrophobic surfaces. Despite the low surface energy of PDMS, the maximum apparent contact angle that can be achieved is only approximately 120° without extra modification.[29] Creating surface roughness can increase the apparent contact angle for superhydrophobicity, but it is challenging to maintain the robustness under external mechanical forces.[30] Efforts to address this challenge have led to the use

[a] CAS Key Laboratory of Design and Assembly of Functional Nanostructures, Fujian Key Laboratory of Nanomaterials, Fujian Institute of Research on the Structure of Matter, Chinese Academy of Sciences, Fuzhou 350002, China. E-mail: lxwu@fjirsm.ac.cn
[b] Fujian Provincial Key Laboratory of Eco-Industrial Green Technology, College of Ecological and Resources Engineering, Wuyi University, 354300, Wuyishan, China
[c] Department of Engineering Science and Mechanics, The Pennsylvania State University, University Park, Pennsylvania 16802, USA. E-mail: huanyu.cheng@psu.edu
[d] School of Chemistry and Chemical Engineering, Guangzhou University, Guangzhou, 510006, P. R. China. E-mail: linjin00112043@126.com, linjing@gzhu.edu.cn

† Electronic supplementary information (ESI) available. See DOI: https://doi.org/10.1039/d3tc01666h

of the desired morphology, *e.g.*, as interconnected microstructures, protecting hydrophobic nanostructures from mechanical damage by objects larger than the framework size.[31] Constructing SH surfaces relies on rough structures and low surface energies.[32] Therefore, multiple methods have been explored to create multiscale structures, including laser irradiation/etching,[33,34] compression molding with templates,[35–37] coating,[38–41] and particle filling.[42,43] However, each method has its own limitations; for example, it is challenging to achieve complicated microstructures with laser processing, an additional compression step is required for templating to avoid damaging the surface morphology during demolding, extra spray coating is needed to improve the durability over time,[44–46] or difficulties are experienced in controlling the surface morphology/adhesion force for particle filling. New strategies have emerged over the years to achieve droplet control. Aizenberg *et al.*[47] introduced adaptive surfaces consisting of a liquid film supported by a nanoporous elastic substrate. These surfaces undergo changes in topography as the substrate deforms, resulting in adjustments in optical transparency and wettability. Wang *et al.*[34] achieved the high-velocity and ultralong transport of droplets by printing surface charge density gradients on various substrates. In addition, Du *et al.*[48,49] enabled the control of droplets in different working scenarios by strategically constructing a photothermal-responsive composite matrix or developing a novel superamphiphobic material with a light-induced surface charge regeneration capability. In our work, we draw inspiration from nature,[50–52] where the presence of anisotropic structures plays a crucial role in determining whether a superhydrophobic surface exhibits the Cassie–Baxter state or the Wenzel state. Mimicking the arc shape of water droplets sagging between protrusions on superhydrophobic surfaces,[53] the incorporation of arc-shaped air pockets with larger cavities proves advantageous in preventing contact with the sagging portion of the droplet. This effectively reduces the overall contact area and helps to maintain the Cassie–Baxter state. By contrast, the presence of V-shaped air pockets is more prone to interacting with the sagging liquid, ultimately leading to the Wenzel state of superhydrophobicity.

This study reports a facile and scalable method to prepare stretchable SiO_2 nanoparticle-modified superhydrophobic PDMS elastomers with periodic surface microstructures (*e.g.*, arc-shaped air pockets and V-shaped air pockets). The different periodic surface microstructures enable the SH PDMS elastomers to either produce a CB-to-W transition or maintain the CB state upon the application of an external pressing force. The resulting SH PDMS elastomers are demonstrated in liquid droplet micro-reactors and transport. The results from this study also provide new design strategies and application opportunities for the SH surfaces with on-demand tunable wettability in stretchable microfluidic devices.

2. Experimental

2.1. Materials

The materials were used as received: PDMS (Sylgard 184 kit, Dow Corning, USA), KH570-modified-SiO_2 (Hebei Qinhe Handi Materials Co. Ltd, China), meshes with grid of 800, 1500 (Shanghai Suyan Cloth Manufacturing Co. Ltd, China), silane coupling agent (Shanghai Senya Lubrication Material Co. Ltd, China), NaOH and phenolphthalein (Sigma-Aldrich, USA), HCl (Xilong Scientific, China), $CuSO_4$ (Aladdin, USA), and methylene blue (MB; Mackin, China).

2.2. Preparation of superhydrophobic PDMS elastomers with microstructures

The Sylgard 184 PDMS base and cross-linker (Dow Corning) were mixed at a 10 : 1 ratio to prepare the prepolymer solution. Next, KH570-modified SiO_2 NPs were added to the prepolymer solution at different weight ratios in the range from 0 to 60% under continuous stirring. After silanizing the mesh of grid 800 (TS) or the mesh of grid 1500 (TW) with a coupling agent spray to provide low surface energies for easy peeling, the resulting mixture was poured into a clean container with a mesh at the bottom. Curing at 50 °C for 120 min and gently peeling off from the iron mesh yielded the SH PDMS.

2.3. Testing of the wettability and adhesion force

The contact angles were measured using Kruss K100 apparatus, where a water droplet of 2 or 5 μL was used for the water contact or sliding angle, respectively. The adhesion forces were measured using a high-sensitivity microelectromechanical system (Data-Physics DCAT 25, Germany) with a water droplet (5 μL) on a metal ring being controlled to contact the surface. The droplet was brought to the surface at a constant speed of 0.2 mm s^{-1} for contacting the surface with a constant force for 0, 1, 3, or 5 min. Next, the droplet was retracted from the surface at a constant speed of 0.1 mm s^{-1}, with the adhesion forces recorded.

Wear-resistance testing. The surface of the SH PDMS elastomers was rubbed with sandpaper (grit no. 320) at a distance of 10 cm each time. The water contact and sliding angles were measured over 50 cycles.

2.4. Transport of water droplets

The water droplet was manipulated using a SINDIN SDC-350 contact angle measuring instrument with a high-speed camera. After placing the water droplet of 10 μL on TS-60 on the platform, TW-60 fixed on an upper needle that was connected to the mobile termination was brought into contact with the water droplet with pressure, followed by retraction.

2.5. Self-cleaning test

After placing phenolphthalein powder on the SH PDMS elastomer, a 1 M NaOH solution was continuously dripped onto the surface to roll off the powders.

2.6. Characterization and imaging

The top and cross-sectional profiles of the SH PDMS elastomers with different microstructures were confirmed using scanning electron microscopy (TESCAN MIRA LMS). The roughness was characterized *via* AFM (Bruker Dimension Icon). The three-dimensional images were obtained using an optical microscope

(Bruker Contour GT K 3D). All optical photos and movies were taken using a mobile phone (iPhone 11, Apple Inc.).

3. Results and discussion

3.1. Design and characterization of the PDMS elastomers with periodic surface microstructures

The stretchable SH PDMS elastomers with tunable wettability were prepared by curing the SiO_2 nanoparticle (NP)-modified PDMS prepolymer on a designed template (Fig. 1a). In brief, KH570-modified SiO_2 NPs of 200 nm diameter (Fig. S1, ESI†) were used to avoid agglomeration in the PDMS prepolymer. Commercial meshes (Shanghai Suyan Screen Products Co., LTD) with two representative microstructures (Fig. S2, ESI†) were first coated with a silane coupling agent to form the TS and TW templates (Fig. S3, ESI†). Curing the SiO_2-modified PDMS prepolymer on the template yields the stretchable SH PDMS elastomer with either an arc-shaped or a V-shaped air pocket morphology.

The water contact angle on the PDMS elastomer increased from the intrinsic value of 118.5° (Fig. S4a, ESI†) to 141.2° after introducing the surface microstructures, which was further increased to 153.9° as the KH570-modified SiO_2 NP weight content was increased from 0 to 60% (TS-60), with the water sliding angle reduced from 40.3° to 9.4° (Fig. 2a). The even distribution of KH570-modified-SiO_2 NPs in the TS-60 PDMS elastomer (Fig. 2b(I)) contributed to an increased roughness of Ra = 78.5 nm (Fig. S5a, ESI†), compared with that of 1.1 nm for the flat PDMS elastomer (Fig. S4b, ESI†). Periodic arc-shaped grooves (air pockets) were formed as shown in Fig. 2b(II). The three-dimensional (3D) profile also shows a roughness of 159.4 μm for the periodic surface microstructures (Fig. 2c). The TS-60 surface with a large contact angle (>150°) and a small sliding angle (<10°) enable rolling off the phenolphthalein powders using 1 M NaOH, producing pink droplets for self-cleaning (Movie S1, ESI†). The high roughness formed with the templates creates a large surface area, which traps air and reduces the contact area between the liquid and the solid surface. In addition, the high aspect ratio of the microstructures helps to maintain the trapped air pockets and prevents them from collapsing.

Using the template TW also increased the water contact angle from 132.9° to 153.1° and decreased the water sliding angle from 58.6° to 9.7° with an increase in the SiO_2 NP weight

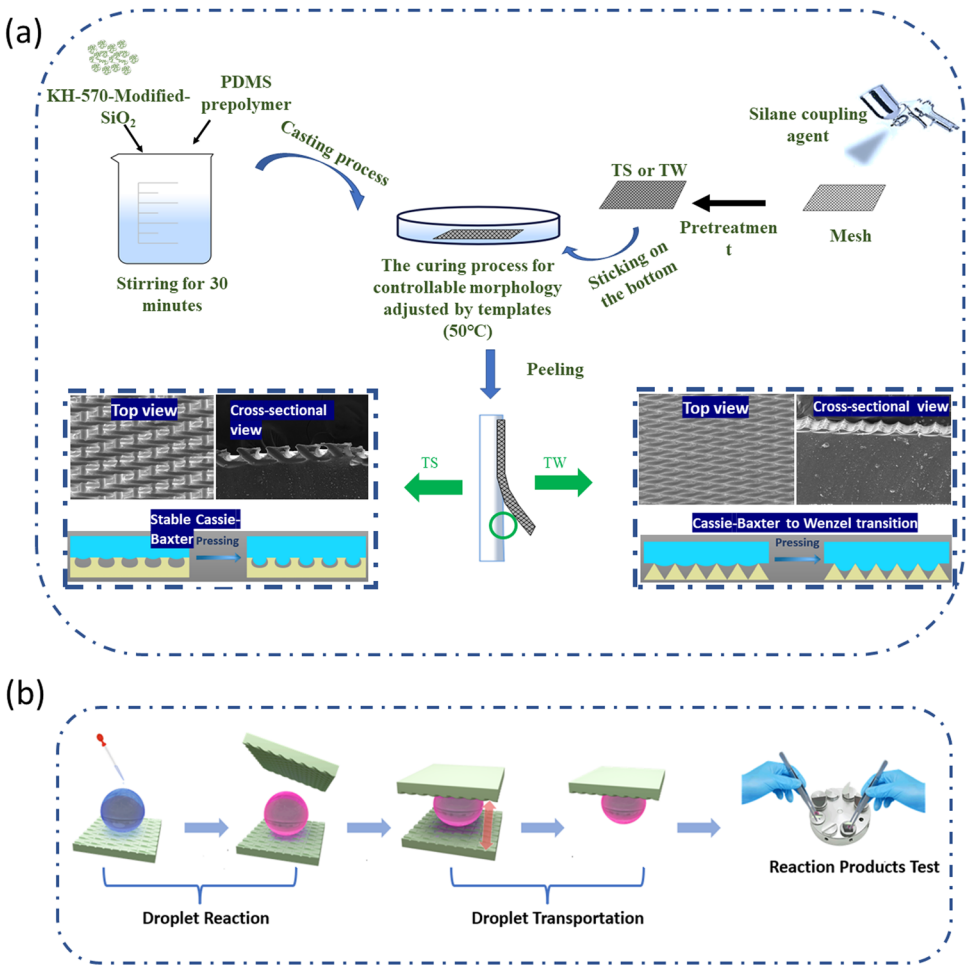

Fig. 1 Overview of the (a) fabrication and (b) application of stretchable superhydrophobic (SH) elastomers with on-demand tunable wettability based on different surface microstructures.

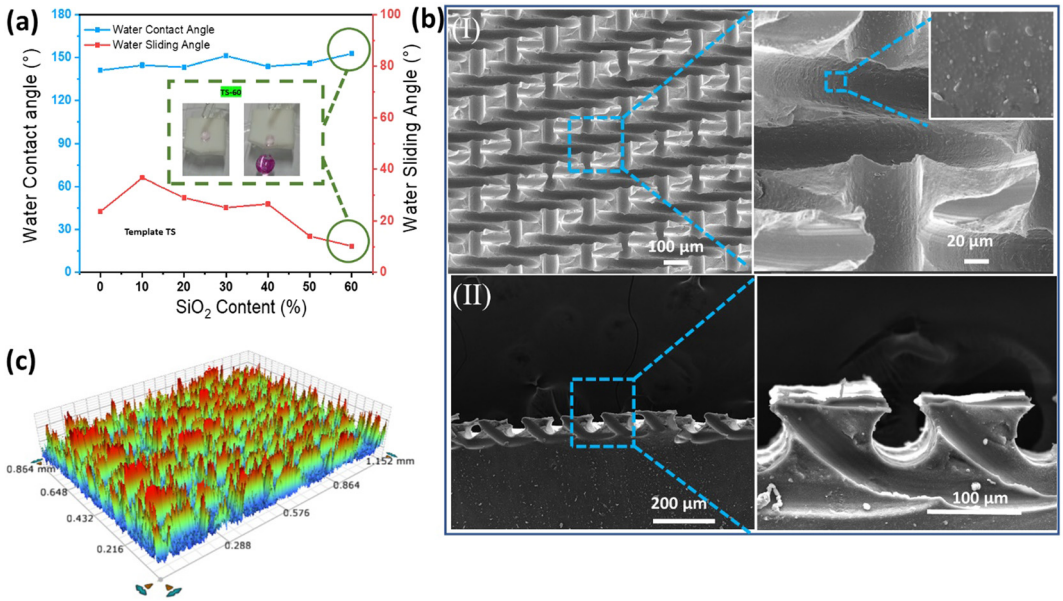

Fig. 2 (a) Dependence of the water contact and sliding angles of the stretchable PDMS elastomer formed by template TS on the SiO_2 content, with images of the self-cleaning test for the TS-60 sample (SiO_2 content: 60%) shown in the inset. (b) Top (top) and cross-sectional (bottom) views of the SEM images of TS-60. (c) Three-dimensional (3D) profile image of TS-60 for an area of 1 mm × 1 mm.

content from 0 to 60% (TW-60) (Fig. 3a). Evenly distributed KH570-modified-SiO_2 NPs in the TW-60 PDMS elastomer (Fig. 3b(I)) also increased the roughness to 74.6 nm (Fig. S5b, ESI†). Periodic V-shaped air pockets were formed, as shown in Fig. 3b(II). A roughness of 124.9 μm was observed in TW-60 with the periodic surface microstructures (Fig. 3c), which is smaller than the surface of TS-60. The excellent superhydrophobic properties of TW-60 are also highlighted by the self-cleaning process (Movie S2, ESI†). The mechanism behind the superhydrophobicity is based on the balance between the interfacial energies of the solid–liquid and solid–air interfaces. When the rough surface is hydrophobic, the surface energy of the solid–liquid interface is high, while the surface energy of the solid–air interface is low. Therefore, the liquid droplet prefers to minimize its contact with the solid surface and instead sits on top of the trapped air pockets, forming a composite interface with the air and the rough surface. Due to the roughness of TS-60 being larger than that of TW-60, we can learn that the U-shaped air pockets are beneficial for increasing the roughness.

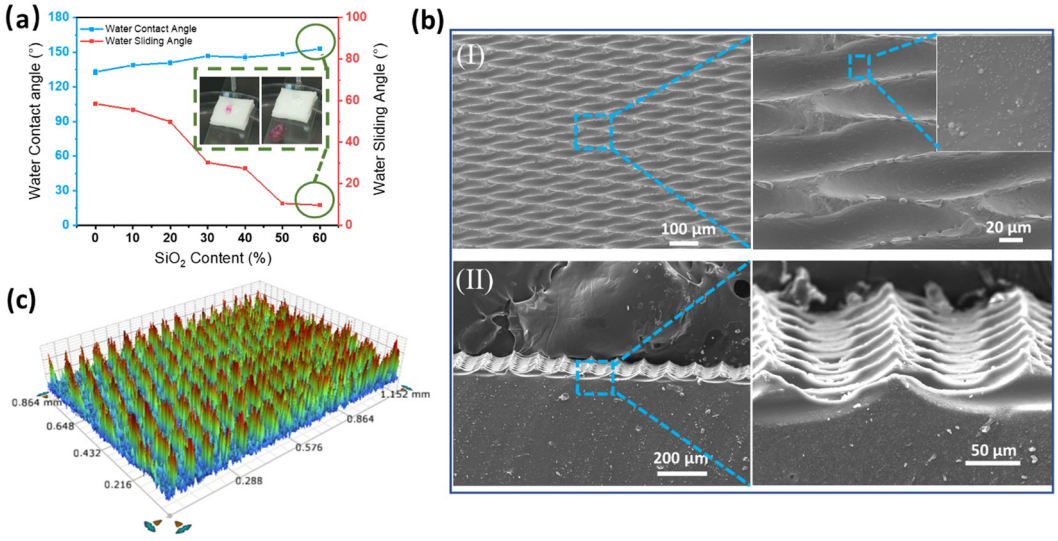

Fig. 3 (a) Dependence of the water contact and sliding angles of the stretchable PDMS elastomer formed by the template TW on the SiO_2 content, with images of the self-cleaning test for the TW-60 sample shown in the inset. (b) Top (top) and cross-sectional (bottom) views of the SEM images of TW-60. (c) 3D profile image of TW-60.

3.2. Stability of the adhesion and mechanical properties of the SH PDMS elastomers

The stability of the surface adhesion can be characterized *via* the liquid standing time on the SH surface. After setting a 10 μL MB droplet (1.0 mM) on the surface of TS-60 (Movie S3, ESI†) and TW-60 (Movie S4, ESI†) for a standing time of 3 s or 1/3/5 min (Fig. 4a), the samples were rotated to observe the rolling behavior of the MB droplet. While TS-60 exhibits easy rolling for all the experiments, rolling only occurs for a standing time of 3 s on the TW-60 sample. The comparison indicates that a CB-to-W transition occurs for TW-60, whereas TS-60 remains in the CB state during the test.

The CB state superhydrophobicity is a phenomenon that is observed when a liquid droplet rests on a rough surface with air trapped in the spaces between the surface asperities. The liquid droplet is suspended on top of the rough surface and only comes into contact with a small fraction of the surface area, resulting in a very high contact angle and a low contact angle hysteresis. This state can be achieved by designing periodic

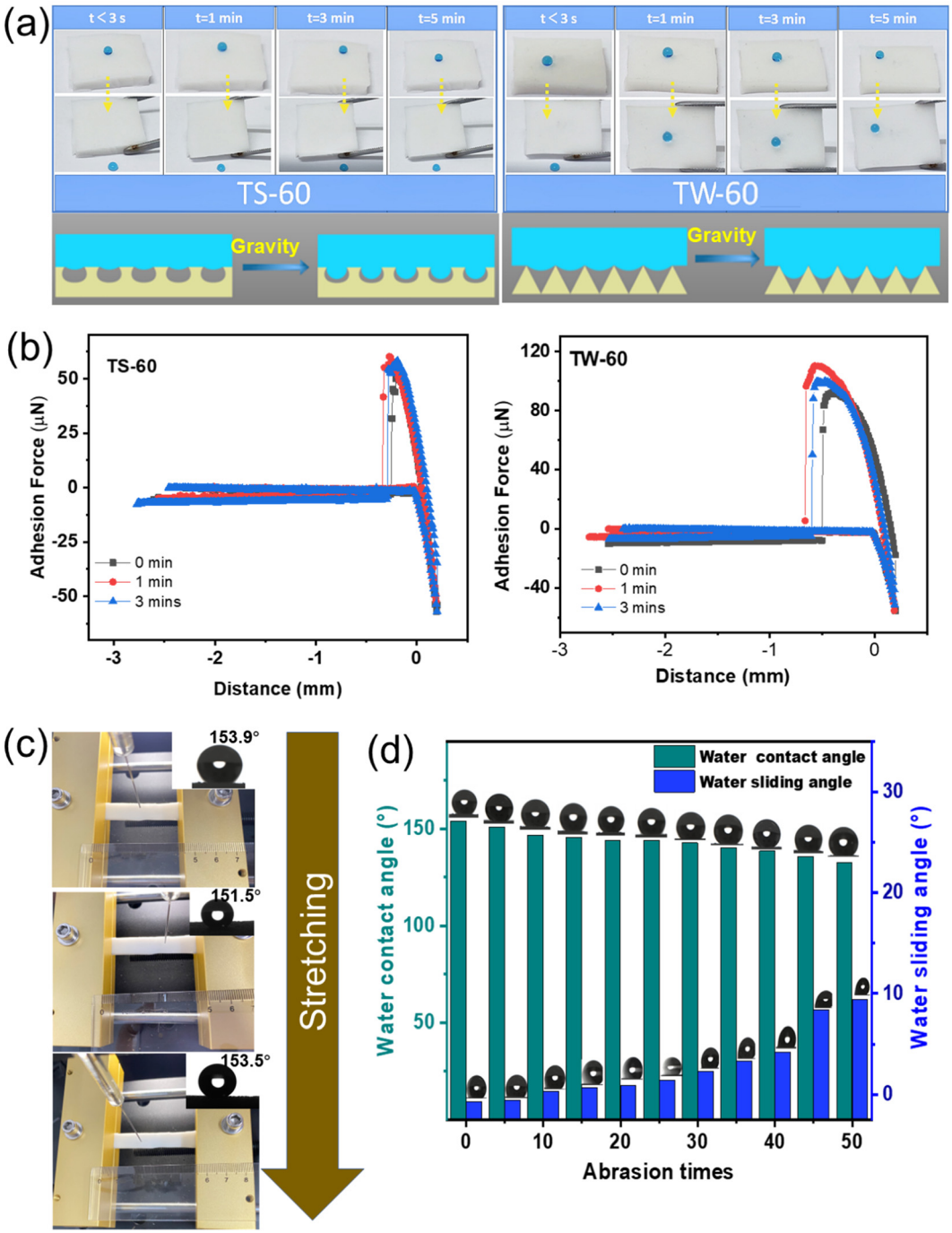

Fig. 4 (a) Stability test of the adhesion force for TS-60 and TW-60. (b) Adhesion force between the water droplet and TS-60 (left) or TW-60 (right) for a pressing time of 0, 1, and 3 min. (c) Stability testing of the water contact angle on TS-60 upon stretching. (d) Wear resistance testing of TS-60.

surface microstructures with a high aspect ratio and a sufficient roughness. The transition from the Cassie–Baxter state to the Wenzel state occurs when the trapped air pockets between the surface asperities are removed and the liquid droplet comes into direct contact with the solid surface.[54] This transition can be induced by changing the surface chemistry of the rough surface or by applying external forces, such as compression.[55] The underlying mechanism for the transition from the Cassie–Baxter state to the Wenzel state is based on the balance between the interfacial energies of the solid–liquid, solid–air, and liquid–air interfaces. In the Cassie–Baxter state, the trapped air pockets reduce the solid–liquid contact area and minimize the solid–liquid interfacial energy, while maximizing the solid–air and liquid–air interfacial energies. When the trapped air pockets are removed or their volume is reduced, the solid–liquid contact area increases, resulting in a decrease in the contact angle and an increase in the contact angle hysteresis. This transition is driven by changing the total interfacial energy, which can be achieved using surface patterning methods, which create specific patterns on the surface can also help to create trapped air pockets. For our samples, as the meniscus radius of the water droplets grows as the standing time increases due to gravity, the internal hydrostatic force increases to be greater than that of the Laplace pressure for triggering the CB-to-W transition on textured polymer surfaces.[55] By contrast, in the case of TS-60, the droplet meniscus grows under gravity without touching the inner surface due to the special arc-shaped air pockets in TS-60 (contrary to TW-60 which has V-shaped air pockets), and thus the CB-to-W transition occurs only in TW-60.

The unique CB-to-W transition in TW-60 is confirmed by testing the adhesion droplet force over time (Fig. 4b). The testing setup and the process are shown in Fig. S6 (ESI†). After the water droplet of 5 μL is brought into contact with the sample surface, a constant force is applied to press and displace it by 0.2 mm. The initial adhesion force of 51.6 μN for TS-60 (91.5 μN for TW-60) increases to 60.3 μN (or 110.4 μN) and then decreases slightly to 58.3 μN (or 99.6 μN) as the pressing time increases to 1 min and then to 3 min. While the slight decrease in the adhesion force for both results from the evaporation of water over time for a reduced contact area, the significantly larger increase for TW-60 comes from the CB-to-W transition.

The mechanical stability of TS-60 is also verified using stretching and wear resistance tests. The transition from the CB to the Wenzel state is often attributed to external stimuli (*e.g.*, mechanical impact, compression, or thermal perturbation) that overcome energy barriers for a given surface topography.[56] The CB equation describes wetting for a two-component surface: $\cos\theta = f_1 \cos\theta_1 + f_2 \cos\theta_2$, where f_1 (or f_2) is the area fraction of the solid (or air) surface in contact with the liquid droplet and θ is the contact angle of the liquid droplet. The increased contact angle and reduced adhesion of the liquid droplet to the surface from an increased f_2 induces a 'sliding effect'.[57] A minimal change in the water contact angle is observed as the TS-60 sample is stretched from 4.5 to 5.0 and then to 5.5 mm (a tensile strain of 111% and 122%, respectively) (Fig. 4c), due to an almost unchanged area fraction of the microstructures during stretching.[56] However, the destruction of the surface microstructure (Fig. S7, ESI†) during sandpaper abrasion for 50 cycles (Fig. S8, ESI†) results in a decreased water contact from 153.9° to 140.3° and an increased water sliding angle from 9.4° to 80.7° (Fig. 4d). We conducted twisting and bending experiments to evaluate the stability of the water contact angle (Fig. S9, ESI†). The procedure involved manually twisting the sample 50 times, followed by bending it 50 times, after which the water contact angle was measured. This cycle was repeated three times. The results indicated that the contact angle remained above 150.0° for both TS-60 and TW-60, indicating that twisting and bending did not compromise the superhydrophobic properties of the prepared samples.

3.3. Transport of water droplets

The difference in the adhesion force between TS-60 and TW-60 under pressure enables the manipulation of water droplets. When compression is applied, the adhesion forces of the TW-60 and TS-60 surfaces are different, which means that the interaction between a water droplet and each surface is different. The water droplet will preferentially adhere to the surface with a higher adhesion force, which means that it will be more difficult to move the droplet away from this surface. By contrast, the surface with a lower adhesion force will have a weaker interaction with the droplet, making it easier to move the droplet away from this surface. As is shown in Fig. 5, the water droplet of 10 μL positioned on TS-60 can be picked up by TW-60 from the above after pressing (Movie S5, ESI†) due to the significantly larger adhesion force on TW-60 from the CB-to-W transition under pressure (Fig. S10a, ESI†). Meanwhile, TS-60 in the CB state (Fig. S10b, ESI†) provides increased pressure in the air pocket between the microstructure and the liquid under pressure according to Boyle's law,[58,59] which can further facilitate the release of the water droplet from the TS-60 surface. When the force is applied to the droplet, it can be moved towards the hydrophobic regions where the adhesion force is lower, and the droplet will be more easily detached from the TS-60 surface with arc-shaped air pockets. In addition, we can learn from the SEM cross-sectional images that the shapes of the air pockets remain unchanged for both TS-60 (Fig. S10c, ESI†) and TW-60 (Fig. S10d, ESI†) after releasing the pressure. Overall, the manipulation of water droplets through differences in the adhesion force relies on

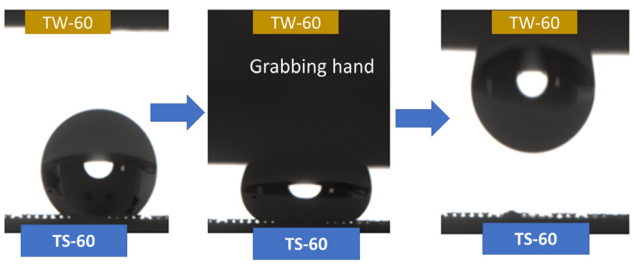

Fig. 5 Transport of a water droplet from TS-60 to TW-60 under pressure.

creating surfaces that have different surface energies in order to create a gradient that controls the movement of the droplets.

3.4. SH PDMS elastomers for multi-stage droplet reactions and droplet transportation

Droplet transportation after multi-stage droplet reactions is important to enable the efficient use of test specimens, to perform a wide range of reactions with different types of reagents and conditions, and to separate incompatible reagents or reaction products. Multi-stage reactions can also enable the production of complex molecules that would be difficult or impossible to synthesize using conventional methods. As shown in Fig. 6, multi-stage droplet reactions can be performed using TS-60 as a liquid microreactor, whereafter TW-60 is used for droplet transportation. The chromogenic reaction between 1.0 M NaOH and phenolphthalein droplets can be readily observed by the instant color change to pink after adding phenolphthalein to the colorless NaOH, followed by the transport of the reaction product by TW-60 (Fig. 6a). Next, adding an HCl droplet into the previous reaction product introduces an acid–base neutralization reaction between H^+ and OH^- to change the droplet back into being colorless, which is followed by another transport step with TW-60 (Fig. 6b). In another demonstration for this liquid microreactor, a precipitation reaction between $CuSO_4$ and NaOH droplets results in the formation of the $Cu(OH)_2$ precipitate, which can also be lifted and transported by TW-60 (Fig. 6c). The stable CB state on TS-60 provides the conditions for the stable droplet reaction, which are attributed to the periodic arc-shaped air pockets. By contrast, the transition from the Cassie–Baxter to the Wenzel state that occurs on TW-60 under an applied pressure offers the possibility for transporting the droplet reaction products, which is attributed to the V-shaped air pockets. These results provide potential application opportunities for droplet

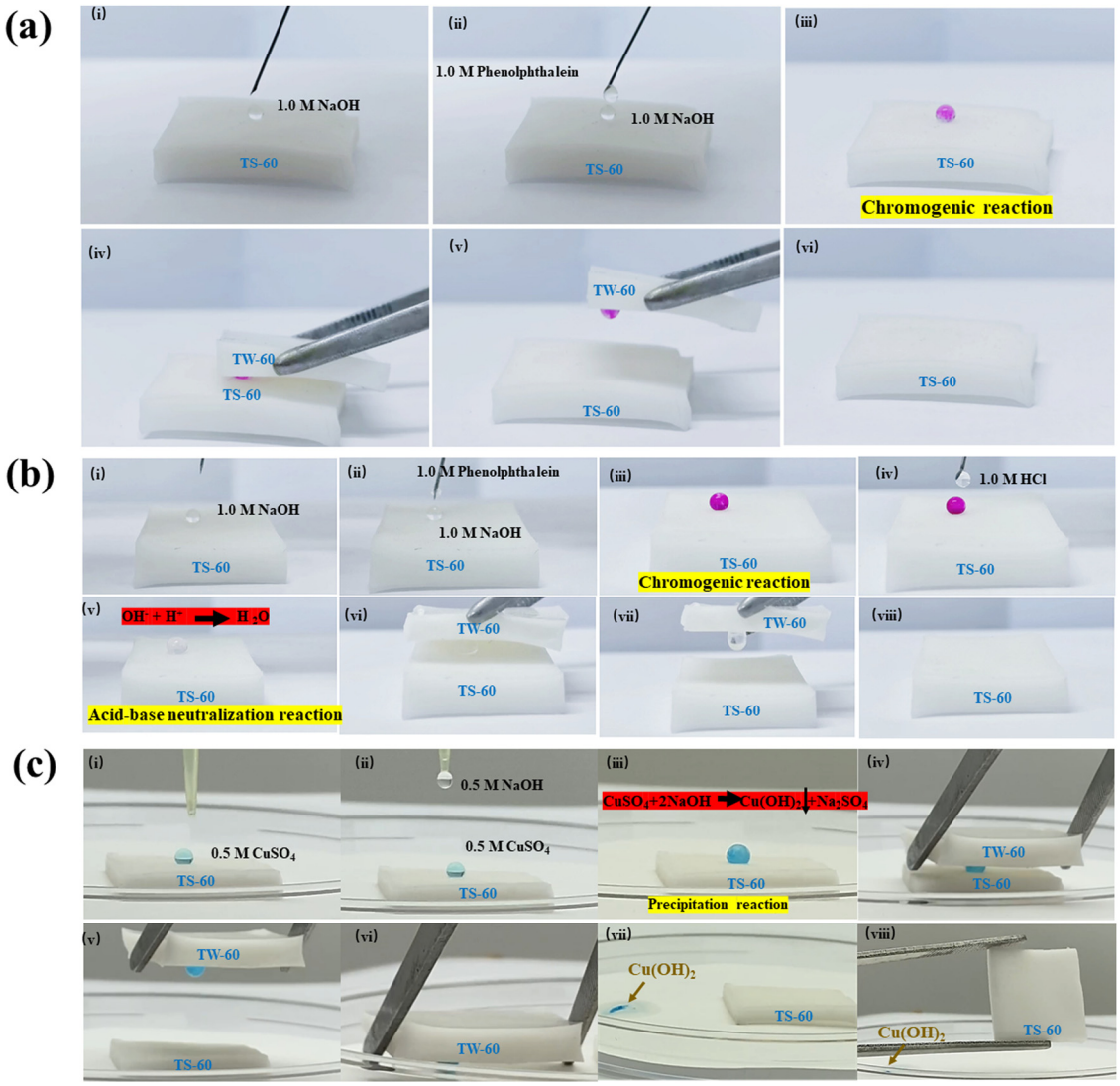

Fig. 6 Application in multi-stage droplet reactions. (a) Chromogenic reaction between the 1.0 M NaOH droplet and the 1.0 M phenolphthalein droplet, followed by transportation with TW-60 (Movie S6, ESI†). (b) Multi-stage chromogenic reactions as in (a) followed by an acid–base neutralization reaction (Movie S7, ESI†). (c) Precipitation reaction followed by transportation using TW-60 (Movie S8, ESI†).

reactions, and the transportation of their products, which can be beneficial for analyzing multi-stage chemical reactions.

4. Conclusions

In summary, this study reports a facile fabrication method to create stretchable SH PDMS elastomers with on-demand, tunable wettability. By combining the KH570-modified-SiO_2 NP-PDMS composite with different microstructure templates, two stretchable superhydrophobic surfaces with different microstructures (arc-shaped or V-shaped air pockets) are formed for use as multi-stage liquid-droplet micro-reactors. The stretchable SH elastomers can either maintain a stable CB state or induce the CB-to-W transition under external triggers such as gravity and pressure. The difference in the adhesion force upon pressure between the two stretchable SH PDMS elastomers enables their utilization in water droplet transport and multi-stage droplet reactions. The low-cost and scalable method also provides the potential applications of digital microfluidics in stretchable devices for biomedical analysis, or biochemical sensing.

Conflicts of interest

There are no conflicts of interest to declare.

Acknowledgements

This study is supported by the National Natural Science Foundation of China (No. 22078077), the Natural Science Foundation of Fujian (No. 2021J05249), the scientific research start-up foundation of Wuyi University (No. YJ202101), a joint funding project for Scientific and Technological Innovation of Nanping (N2020Z015, N2021Z008), the major science and technology project of Fujian province (Grant No.: 2021HZ027003), and the STS Project of Fujian-CAS (Grant No.: 2022T3059, 2022T3003, 2021T3053).

References

1 A. C. Lima and J. F. Mano, Micro/nano-structured superhydrophobic surfaces in the biomedical field: part II: applications overview, *Nanomedicine*, 2015, **10**(2), 271–297.
2 S. Hu, Z. Shi, R. Zheng, W. Ye, X. Gao, W. Zhao and G. Yang, Superhydrophobic Liquid–Solid Contact Triboelectric Nanogenerator as a Droplet Sensor for Biomedical Applications, *ACS Appl. Mater. Interfaces*, 2020, **12**(36), 40021–40030.
3 J. Marlena, J. K. S. Tan, Z. Lin, D. X. Li, B. Zhao, H. L. Leo, S. Kim and C. H. Yap, Monolithic polymeric porous superhydrophobic material with pneumatic plastron stabilization for functionally durable drag reduction in blood-contacting biomedical applications, *NPG Asia Mater.*, 2021, **13**(1), 58.
4 A. Riveiro, T. Abalde, P. Pou, R. Soto, J. del Val, R. Comesaña, A. Badaoui, M. Boutinguiza and J. Pou, Influence of laser texturing on the wettability of PTFE, *Appl. Surf. Sci.*, 2020, **515**, 145984.
5 C. Xu, R. Feng, F. Song, X.-L. Wang and Y.-Z. Wang, Desert Beetle-Inspired Superhydrophilic/Superhydrophobic Patterned Cellulose Film with Efficient Water Collection and Antibacterial Performance, *ACS Sustainable Chem. Eng.*, 2018, **6**(11), 14679–14684.
6 Y. Fan, S. Li, D. Wei, Z. Fang, Z. Han and Y. Liu, Bioinspired Superhydrophobic Cilia for Droplets Transportation and Microchemical Reaction, *Adv. Mater. Interfaces*, 2021, **8**(24), 2101408.
7 S. Shin, J. Lee, S. Lee, H. Kim, J. Seo, D. Kim, J. Hong, S. Lee and T. Lee, A Droplet-Based High-Throughput SERS Platform on a Droplet-Guiding-Track-Engraved Superhydrophobic Substrate, *Small*, 2017, **13**(7), 1602865.
8 N. S. Singh, J. Zhang, J. Stafford, C. Anthony and N. Gao, Implementing Superhydrophobic Surfaces within Various Condensation Environments: A Review, *Adv. Mater. Interfaces*, 2021, **8**(2), 2001442.
9 M. D. Mulroe, B. R. Srijanto, S. F. Ahmadi, C. P. Collier and J. B. Boreyko, Tuning Superhydrophobic Nanostructures To Enhance Jumping-Droplet Condensation, *ACS Nano*, 2017, **11**(8), 8499–8510.
10 X. Lai, Z. Pu, H. Yu and D. Li, Inkjet Pattern-Guided Liquid Templates on Superhydrophobic Substrates for Rapid Prototyping of Microfluidic Devices, *ACS Appl. Mater. Interfaces*, 2020, **12**(1), 1817–1824.
11 Z. Dong, M. Vuckovac, W. Cui, Q. Zhou, R. H. A. Ras and P. A. Levkin, 3D Printing of Superhydrophobic Objects with Bulk Nanostructure, *Adv. Mater.*, 2021, **33**(45), 2106068.
12 D. Lv, S. Li, J. Wan, J. Dong and J. Liu, Bioinspired hierarchically hairy particles for robust superhydrophobic coatings via a droplet dynamic template method, *Polym. Chem.*, 2019, **10**(3), 331–335.
13 S. Wang, K. Liu, X. Yao and L. Jiang, Bioinspired Surfaces with Superwettability: New Insight on Theory, Design, and Applications, *Chem. Rev.*, 2015, **115**(16), 8230.
14 S. Zhang, J. Huang, Z. Chen and Y. J. S. Lai, Bioinspired special wettability surfaces: from fundamental research to water harvesting applications, *Small*, 2017, **13**(3), 1602992.
15 A. Marmur, The Lotus Effect: Superhydrophobicity and Metastability, *Langmuir*, 2004, **20**(9), 3517–3519.
16 E. Bittoun and A. Marmur, The Role of Multiscale Roughness in the Lotus Effect: Is It Essential for Super-Hydrophobicity?, *Langmuir*, 2012, **28**(39), 13933–13942.
17 L. Feng, Y. Zhang, J. Xi, Y. Zhu, N. Wang, F. Xia and L. Jiang, Petal Effect: A Superhydrophobic State with High Adhesive Force, *Langmuir*, 2008, **24**(8), 4114–4119.
18 Y. Shao, J. Zhao, Y. Fan, Z. Wan, L. Lu, Z. Zhang, W. Ming and L. Ren, Shape memory superhydrophobic surface with switchable transition between ''Lotus Effect'' to ''Rose Petal Effect'', *Chem. Eng. J.*, 2020, **382**, 122989.
19 A. Lafuma and D. Quéré, Superhydrophobic states, *Nat. Mater.*, 2003, **2**(7), 457–460.
20 L. Wang, Z. Tian, G. Jiang, X. Luo, C. Chen, X. Hu, H. Zhang and M. Zhong, Spontaneous dewetting transitions of droplets during icing & melting cycle, *Nat. Commun.*, 2022, **13**(1), 378.
21 S. Hoshian, V. Jokinen, K. Hjort, R. H. A. Ras and S. Franssila, Amplified and Localized Photoswitching of

TiO2 by Micro- and Nanostructuring, *ACS Appl. Mater. Interfaces*, 2015, **7**(28), 15593–15599.

22 H. Wu, S. Yu, Z. Xu, B. Cao, X. Peng, Z. Zhang, G. Chai and A. Liu, Theoretical and Experimental Study of Reversible and Stable Wetting States of a Hierarchically Wrinkled Surface Tuned by Mechanical Strain, *Langmuir*, 2019, **35**(21), 6870–6877.

23 M. Umlandt, A. Kopyshev, S. V. Pasechnik, A. V. Zakharov, N. Lomadze and S. Santer, Light-Triggered Manipulations of Droplets All in One: Reversible Wetting, Transport, Splitting, and Merging, *ACS Appl. Mater. Interfaces*, 2022, **14**(36), 41412–41420.

24 C. Yang, Q. Zeng, J. Huang and Z. Guo, Droplet manipulation on superhydrophobic surfaces based on external stimulation: A review, *Adv. Colloid Interface Sci.*, 2022, **306**, 102724.

25 J. Zhang, X. Wang, Z. Wang, S. Pan, B. Yi, L. Ai, J. Gao, F. Mugele and X. Yao, Wetting ridge assisted programmed magnetic actuation of droplets on ferrofluid-infused surface, *Nat. Commun.*, 2021, **12**(1), 7136.

26 E. J. Falde, S. T. Yohe, Y. L. Colson and M. W. Grinstaff, Superhydrophobic materials for biomedical applications, *Biomaterials*, 2016, **104**, 87–103.

27 L. Wang, K. Wang, Z. Lou, K. Jiang and G. Shen, Plant-Based Modular Building Blocks for ''Green'' Electronic Skins, *Adv. Funct. Mater.*, 2018, **28**(51), 1804510.

28 P. Mostafalu, A. S. Nezhad, M. Nikkhah and M. Akbari, in Flexible Electronic Devices for Biomedical Applications, *Advanced Mechatronics and MEMS Devices II*, ed. D. Zhang, B. Wei, Springer International Publishing, Cham, 2017, pp. 341–366.

29 M. P. Wolf, G. B. Salieb-Beugelaar and P. Hunziker, PDMS with designer functionalities—Properties, modifications strategies, and applications, *Prog. Polym. Sci.*, 2018, **83**, 97–134.

30 X. Tian, T. Verho and R. H. A. Ras, Moving superhydrophobic surfaces toward real-world applications, *Science*, 2016, **352**(6282), 142–143.

31 D. Wang, Q. Sun, M. J. Hokkanen, C. Zhang, F.-Y. Lin, Q. Liu, S.-P. Zhu, T. Zhou, Q. Chang, B. He, Q. Zhou, L. Chen, Z. Wang, R. H. A. Ras and X. Deng, Design of robust superhydrophobic surfaces, *Nature*, 2020, **582**(7810), 55–59.

32 S. Parvate, P. Dixit and S. Chattopadhyay, Superhydrophobic Surfaces: Insights from Theory and Experiment, *J. Phys. Chem. B*, 2020, **124**(8), 1323–1360.

33 H. He, W. Wu, Z. Xi, Z. Ma, L. Zhang, C. Wang and L. J. A. S. S. Sun, Time dependency of superhydrophilic and superhydrophobic surfaces produced by nanosecond laser irradiation assisted by post-annealing and silanization, *Appl. Surf. Sci.*, 2022, **586**, 152819.

34 Q. Sun, D. Wang, Y. Li, J. Zhang, S. Ye, J. Cui, L. Chen, Z. Wang, H.-J. Butt, D. Vollmer and X. Deng, Surface charge printing for programmed droplet transport, *Nat. Mater.*, 2019, **18**(9), 936–941.

35 Q. Wen and Z. J. C. L. Guo, Recent advances in the fabrication of superhydrophobic surfaces, *Chem. Lett.*, 2016, **45**(10), 1134–1149.

36 Y. Wu, Z. Wang, J. Yang, H. Song, J. Li, M. Al Kobaisi, Y. T. Dang, D. Zhang, V. K. J. C. Truong, S. A. Physicochemical and E. Aspects, Designing superhydrophobic robotic surfaces: Self-cleaning, high-grip impact, and bacterial repelling, *Colloids Surf., A*, 2021, **629**, 127444.

37 Y. Zhang, Z. Liu, A. Chen, Q. Wang, J. Zhang, C. Zhao, J. Xu, W. Yang, Y. Peng and Z. J. T. Zhang, Fabrication of micro-/submicro-/nanostructured polypropylene/graphene superhydrophobic surfaces with extreme dynamic pressure resistance assisted by single hierarchically porous anodic aluminum oxide template, *J. Phys. Chem. C*, 2020, **124**(11), 6197–6205.

38 N. Celik, I. Torun, M. Ruzi, A. Esidir and M. S. Onses, Fabrication of robust superhydrophobic surfaces by one-step spray coating: Evaporation driven self-assembly of wax and nanoparticles into hierarchical structures, *Chem. Eng. J.*, 2020, **396**, 125230.

39 T. Verho, C. Bower, P. Andrew, S. Franssila, O. Ikkala and R. H. A. Ras, Mechanically Durable Superhydrophobic Surfaces, *Adv. Mater.*, 2011, **23**(5), 673–678.

40 Y. Zhou, Y. Ma, Y. Sun, Z. Xiong, C. Qi, Y. Zhang and Y. Liu, Robust Superhydrophobic Surface Based on Multiple Hybrid Coatings for Application in Corrosion Protection, *ACS Appl. Mater. Interfaces*, 2019, **11**(6), 6512–6526.

41 Z. Wang, X. Liu, J. Ji, T. Tao, T. Zhang, J. Xu, Y. Jiao and K. Liu, Underwater Drag Reduction and Buoyancy Enhancement on Biomimetic Antiabrasive Superhydrophobic Coatings, *ACS Appl. Mater. Interfaces*, 2021, **13**(40), 48270–48280.

42 J. Yang, P. Pi, X. Wen, D. Zheng, M. Xu, J. Cheng and Z. Yang, A novel method to fabricate superhydrophobic surfaces based on well-defined mulberry-like particles and self-assembly of polydimethylsiloxane, *Appl. Surf. Sci.*, 2009, **255**(6), 3507–3512.

43 J. Zhao, X. Gao, S. Chen, H. Lin, Z. Li and X. Lin, Hydrophobic or superhydrophobic modification of cement-based materials: A systematic review, *Composites, Part B*, 2022, **243**, 110104.

44 S. Ramakrishna, D. Mathew and K. S. Santhosh Kumar, Self-assembled and elastomeric arm decorated surfaces for high stress resistant super-repellent materials, *J. Mater. Chem. A*, 2017, **5**(2), 699–711.

45 B. Wu, C. Peng, Y. Hu, S. Xing, D. Jiang, J. Yang, J. Lyu and Y. He, Molding processed multi-layered and multi-functional nanocomposites with high structural ability, electrical conductivity and durable superhydrophobicity, *Nanoscale*, 2018, **10**(42), 19916–19926.

46 A. Milionis, E. Loth and I. S. Bayer, Recent advances in the mechanical durability of superhydrophobic materials, *Adv. Colloid Interface Sci.*, 2016, **229**, 57–79.

47 X. Yao, Y. Hu, A. Grinthal, T.-S. Wong, L. Mahadevan and J. Aizenberg, Adaptive fluid-infused porous films with tunable transparency and wettability, *Nat. Mater.*, 2013, **12**(6), 529–534.

48 F. Wang, M. Liu, C. Liu, Q. Zhao, T. Wang, Z. Wang and X. Du, Light-induced charged slippery surfaces, *Sci. Adv.*, 2022, **8**(27), eabp9369.

49 F. Wang, M. Liu, C. Liu, C. Huang, L. Zhang, A. Cui, Z. Hu and X. Du, Light control of droplets on photo-induced charged surfaces, *Nat. Sci. Rev.*, 2023, **10**(1), nwac164.
50 S. Zhu, Y. Bian, T. Wu, C. Chen, Y. Jiao, Z. Jiang, Z. Huang, E. Li, J. Li, J. Chu, Y. Hu, D. Wu and L. Jiang, High Performance Bubble Manipulation on Ferrofluid-Infused Laser-Ablated Microstructured Surfaces, *Nano Lett.*, 2020, **20**(7), 5513–5521.
51 S. Jiang, Y. Hu, H. Wu, Y. Zhang, Y. Zhang, Y. Wang, Y. Zhang, W. Zhu, J. Li, D. Wu and J. Chu, Multifunctional Janus Microplates Arrays Actuated by Magnetic Fields for Water/Light Switches and Bio-Inspired Assimilatory Coloration, *Adv. Mater.*, 2019, **31**(15), 1807507.
52 Z. Cui, L. Xiao, Y. Li, Y. Zhang, G. Li, H. Bai, X. Tang, M. Zhou, J. Fang, L. Guo, S. Liu, C. Xiao and M. Cao, A fishbone-inspired liquid splitter enables directional droplet transportation and spontaneous separation, *J. Mater. Chem. A*, 2021, **9**(15), 9719–9728.
53 E. Bormashenko, Progress in understanding wetting transitions on rough surfaces, *Adv. Colloid Interface Sci.*, 2015, **222**, 92–103.
54 T. Baldacchini, J. E. Carey, M. Zhou and E. Mazur, Superhydrophobic Surfaces Prepared by Microstructuring of Silicon Using a Femtosecond Laser, *Langmuir*, 2006, **22**(11), 4917–4919.
55 D. Murakami, H. Jinnai and A. Takahara, Wetting Transition from the Cassie–Baxter State to the Wenzel State on Textured Polymer Surfaces, *Langmuir*, 2014, **30**(8), 2061–2067.
56 B. Liu and F. F. Lange, Pressure induced transition between superhydrophobic states: Configuration diagrams and effect of surface feature size, *J. Colloid Interface Sci.*, 2006, **298**(2), 899–909.
57 J. Macko, N. Podrojková, R. Oriňaková and A. Oriňak, New insights into hydrophobicity at nanostructured surfaces: Experiments and computational models, *Nanomater. Nanotechnol.*, 2022, 12.
58 Y. Lai, X. Gao, H. Zhuang, J. Huang, C. Lin and L. Jiang, Designing Superhydrophobic Porous Nanostructures with Tunable Water Adhesion, *Adv. Mater.*, 2009, **21**(37), 3799–3803.
59 J. B. West, The original presentation of Boyle's law, *J. Appl. Physiol.*, 1999, **87**(4), 1543–1545.

